Experimental study of the efficiency of a SDD X-ray detector by means of PIXE spectra

S. Limandri,[a]* G. Bernardi[a,b] and S. Suárez[a,c]

The efficiency of a silicon drift detector with ultrathin window was studied for energies between 0.27 and 25 keV. Experimental values of the X-ray yields from samples of known stoichiometry were obtained by impact of 2 MeV protons. By using theoretical calculations of these yields the relative efficiency of the detector was evaluated. The results are compared with efficiency values obtained from the window transmission and the detector quantum efficiency. A quantitative analysis of a particle induced X-ray emission spectrum for a reference sample was performed in order to evaluate the consistency of the data presented in this work. Copyright © 2013 John Wiley & Sons, Ltd.

Introduction

Silicon drift detectors (SDD) were first developed in the 1980s and are used nowadays in analytical techniques such as X-ray fluorescence, electron prove microanalysis, and particle induced X-ray emission (PIXE). These detectors are derived from the principle of sideward depletion and consist of a cylinder of high resistivity n-type silicon fully depleted by reverse biased p+ junctions covering both surfaces. Initially, the electric field was achieved by segmentation of the p+ regions on both surfaces forming patterns of parallel strips and superposition of a voltage gradient.[1] Later, to optimize the SDD for X-ray spectroscopy, the strip system in one of the surfaces was replaced by a large area p+ junction, which acts as a thin radiation entrance window.[2] A further improvement consisted in using circular p+ strips on the other surface and placing the small sized n+ anode in the center of this layer. In this configuration, charge carrier trajectories are parallel to the detector surface because of a radial electric field. The anode is connected directly to an integrated junction field-effect transistor, which acts as a current preamplifier. The low capacitance of the anode permits to improve the energy resolution and to operate the SDD at pulse shaping time constants 100 times lower than the ones used in conventional solid state detectors. This means that the SDD can be used at higher counting rates of the incident photons. Although the SDD can operate at room temperature, the best performance is obtained by cooling it down to −20 °C (Peltier cooling). On the low energy region, the quantum efficiency (QE) of the detector depends on the entrance window technology[3,4] and on the high energy it is given by the full depletion thickness of the silicon.

The counting efficiency is an important feature of an energy dispersive detection system. It affects the performance of the measurement process and the total counting time.[5] For quantification without standards in materials analysis, the knowledge of the detector efficiency is a key issue. The detector efficiency is composed of two factors, the geometric and the intrinsic efficiency. The geometric contribution is given by the fraction of the solid angle subtended by the X-ray detector. The intrinsic efficiency ε is related to the transmission through the entrance window, the contact layer, and any possible additional absorbing layers up to the active detector volume. It also depends on the detector thickness, and it may be affected by the electronic pulse processing.[6] At low photon energies, the intrinsic efficiency is highly influenced by the absorption in the entrance window, leading to a strong decrease in the efficiency below 2 keV. Then, quantification of X-ray spectra of samples containing light elements can be affected by large uncertainties if the efficiency is not properly known.

Different approaches have been proposed to determine the detector efficiency. Tschischgale et al.[7] determined the efficiency of a Si(Li) detector at low energies by comparing the electron bremsstrahlung spectra for bulk samples with theoretical predictions. Tribedi and Tandon[8] obtained the intrinsic efficiency of a Si(Li) detector in the range of 1–20 keV by using radioactive sources and complemented the data at lower energies by using PIXE spectra from thin films. Scholze and Ulm[9] measured the efficiency of a windowless Si(Li) detector by means of synchrotron radiation. Alvisi et al.[10] developed a methodology to determine the efficiency of an energy dispersive spectrometer (EDS) on the basis of the comparison between X-ray emission spectra from a reference sample measured in a calibrated EDS and with the EDS whose efficiency wants to be determined. The calibration of the EDS was performed by means of synchrotron radiation. Even when the method was applied for electron excited spectra, it could be easily extended to other excitation sources. Nevertheless, many research centers do not have a calibrated detector. In this case, the reference spectrum acquired with the calibrated detector must be provided. In addition, this spectrum must be obtained with

---

* Correspondence to: S. Limandri, Consejo Nacional de Investigaciones Científicas y Técnicas (CONICET), Buenos Aires, Argentina. E-mail: limandri@cab.cnea.gov.ar

a Consejo Nacional de Investigaciones Científicas y Técnicas (CONICET), Buenos Aires, Argentina

b Centro Atómico Bariloche, Comisión Nacional de Energía Atómica, Bustillo 9500, San Carlos de Bariloche, Río Negro, Argentina

c Instituto Balseiro, Universidad Nacional de Cuyo, Bustillo 9500, San Carlos de Bariloche, Río Negro, Argentina

487

the same excitation source to be used with the detector of unknown efficiency.

In this work, we determined the intrinsic efficiency of an SDD with ultrathin window in the energy range between 0.27 and 25 keV by comparing the characteristic X-ray intensities induced by proton impact on bulk samples with theoretical predictions of the yields. The values obtained were compared with estimations of the efficiency based on the window transmission and the detector QE. The consistency of the data obtained is evaluated by performing a quantification without standards of an X-ray spectrum for a sample of known composition.

The intrinsic efficiency

The intrinsic efficiency $\varepsilon(E)$, as a function of the photon energy E, is the probability that a photon can go through the entrance window and the inactive layers of the detector and be absorbed in the active zone. It can be written as

$$\varepsilon(E) = T_{win}(E)\, QE(E) \tag{1}$$

where $T_{win}(E)$ is the transmission of the entrance window, and QE is the detector quantum efficiency. The factors $T_{win}(E)$ and QE(E) are expressed as[6]

$$T_{win}(E) = e^{-(\mu\rho x)_{win}}\left[f_{O.A} + (1 - f_{O.A})e^{-\mu_{Si}\rho_{Si}x_{grid}}\right] \tag{2}$$

$$QE(E) = e^{-(\mu\rho x)_{OH}}e^{-(\mu\rho x)_{DL}}\left(1 - e^{-(\mu\rho x)_{det}}\right)(1 - \eta) \tag{3}$$

where $(\mu\rho x)_i$ is the product of the X-ray mass absorption coefficient, the mass density, and the thickness of the i-th layer of the detector; $f_{O.A}$ and x_{grid} are, respectively, the fraction of the open area and the thickness of the supporting grid; and η is the Si escape peak probability.[11] The subindexes grid, win, OH, DL and det refer to the supporting grid, the entrance window, the ohmic contact, the dead layer, and the detector crystal, respectively.

Determination of the intrinsic efficiency from X-ray spectra

The approach proposed here to estimate the intrinsic efficiency from X-ray emission spectra is based on the comparison between experimental intensities and theoretical predictions. For proton excitation of a bulk homogeneous sample without secondary X-ray fluorescence effects, the intensity I_j of the X-ray characteristic K line of the element j is[12]

$$I_j = \frac{N_A}{A_j}\omega_{k,j}b_{k,j}\frac{\Delta\Omega}{4\pi}N_pC_j\varepsilon_j\int_{E_o}^{0}\frac{\sigma_j(E)T_j(E)}{S_M(E)}dE \tag{4}$$

N_A being the Avogadro'constant A_j, the atomic weight; ω_{kj}, the fluorescence yield for the K shell; b_{kj}, the relative transition probability of the considered line; $\Delta\Omega$, the solid angle subtended by the X-ray detector; N_p, the number of incident protons; C_j, the concentration of the j-th element; ε_j, the intrinsic efficiency of the X-ray detector at the X-ray energy of the considered line; σ_j, the ionization cross section; S_M, the stopping power of the ions in the sample; and T_j, the transmission factor of photons. For L or higher line excitation, the expression for the characteristic intensity is similar to Eqn (4), but the ionization cross section is replaced by the vacancy production cross section (which takes

into account vacancies generation due to Coster–Kronig transitions). To simplify the notation, the Eqn (4) is written as follows:

$$I_j = \varepsilon_j\Delta\Omega Y_j \tag{5}$$

The factor Y_j is known as X-ray yield[12] and corresponds to the total production of photons of the considered line per unit of solid angle emitted by the j-element of the sample. This factor depends on the considered element and on the whole matrix.

By making the ratio between the X-ray intensity corresponding to characteristic lines of two elements (a, b) in the sample, we obtain the ratio of the efficiency at two different photon energies E_a and E_b:

$$\frac{\varepsilon_a}{\varepsilon_b} = \frac{I_a}{I_b}\frac{Y_b}{Y_a} \tag{6}$$

If the value of the efficiency at the energy E_b is known, then the value at the energy E_a can be derived by measuring the intensities and calculating the theoretical yields. Additionally, we note that in the expression of the efficiency ratio, some experimental parameters (number of incident protons and solid angle subtended by the X-ray detector) cancel out. This procedure reduces errors that are coming from the uncertainty of the cancelled out parameters. For example, the solid angle subtended by the X-ray detector is determined by the sample-detector distance, the beam spot diameter, and the effective detector area,[13] which are difficult to determine with good precision. Besides, the accumulated charge is usually collected from the sample holder. Unfortunately, secondary electrons that escape from the sample can cause an overestimation of the total charge.[14]

In the case of mono-elemental samples, the efficiency ratio can be performed for emission lines corresponding to different groups (K, L, or M). In this case, the concentration of the involved element is also cancelled out when making the ratio.

Experimental

X-ray emission spectra from bulk samples were acquired for SiO_2, $CaCO_3$ (in two forms: a crystal rock and a pellet done with commercial powder), $NaAlSi_3O_8$, Al_2O_3, $GaAs$, FeS_2, CaF_2, Fe_3O_4, ZnS, $BaSO_4$, Pd, Mo, Ta, Hf, W, and Ta. The measurements were performed at Centro Atómico Bariloche in the 1.7 MV Tandem accelerator provided with a microbeam line and an RC43 endstation from the National Electrostatic Corporation. We used a 2 MeV proton beam of 2 mm diameter, with a current of 2 nA to collect a total charge of 1 μC for each spectrum. The total charge delivered to the sample was measured with a current integrator from the total current in both, the sample holder, and the vacuum chamber, which are electrically connected.

An additional spectrum corresponding to a press pellet of a sample with a known composition was also measured under the same conditions in order to verify the consistency of the efficiency values obtained in this work. The oxide composition of this reference sample was determined by Actlabs[15] by fusion inductively coupled plasma. The elemental composition was deduced from the stoichiometric formulas, and the carbon concentration was estimated as the loss of ignition amount.

The X-ray detector is an SDD e2v SiriusSD® with ultrathin polymer window, with 30 mm^2 nominal area placed at 15 cm from the sample (solid angle of 1.33 10^{-3} srad). According to the data

provided by the manufacturer, the ultrathin window Moxtek AP3.3 has a 380-μm-thick silicon support structure with a 77% open area and a 300 nm polymer layer. The detector has an aluminum electric contact (30 nm thick) and an active zone of 0.045 cm. The detector itself has a so-called 'pn entrance layer'. A pn-window refers to the implantation of boron ions through a SiO_2 layer at the radiation entrance zone. This reduces the width of the partially insensitive area caused by the highly p+ dopped region at the entrance zone, minimizing the recombination, and, consequently, the loss of signal carriers.[4] This technology allows to obtain more symmetric low X-ray energy peaks, improving the energy resolution.[5]

Results and discussion

In Fig. 1, we show QE as a function of the X-ray energy, including data provided by the manufacturer and our calculations with Eqn (3), for a detector with a standard and a pn entrance layer. The calculations were performed using the nominal thicknesses of the ohmic, dead, and active layers composing the detector and the absorption coefficients given by Chantler *et al.*[16] For a detector with a standard front layer, the calculated curve agrees very well with the data provided by the manufacturer, except for energies larger than 10 keV.

In the case of a detector with a pn-window, at low photon energies, the QE is lower than the one corresponding to a detector with a standard entrance layer. Even when the efficiency is lower, the pn-window minimizes the loss of electrons generated in the p+ layer located at the entrance zone of the radiation. In this configuration, the incomplete charge collection effect is lower, improving the resolution at low energies.[5]

We observed in Fig. 1 that the steps in the QE curve for the detector with a pn entrance layer are due to the presence of Si and O. Then, we tried to reproduce these results by adding a layer of SiO_2 in Eqn (3) and optimizing the mass thickness to fit the curve provided by the manufacturer. A good agreement is obtained for a mass thickness of 9 μg/cm² or a linear thickness of 34 nm assuming a SiO_2 density equal to the bulk density, i.e. 2.65 g/cm³.

In Fig. 1, the decreasing behavior of the QE for energies larger than 10 keV is independent of the entrance layer for our calculations and for the data given by the supplier. In this energy range, QE is mainly dominated by the energy dependence of the silicon mass absorption coefficient [Eqn (3)]. Then, we attributed the observed differences between the calculations and the supplier data to the database used for mass absorption coefficients.

In Fig. 2, we show the data and calculations of the window transmission T_{win} as function of the X-ray energy. Scholze and Procop measured the transmission of a Moxtek AP3.3 window by means of synchrotron radiation and interpolated the experimental data by using several databases for mass absorption coefficients.[6] The curve corresponding to these authors was obtained using the mass thicknesses and the elements given in Table 1 of their article and the X-ray mass absorption coefficients given by Chantler *et al.*[16] The resulting transmission curve is in good agreement with the data given by the window supplier,[17] as shown in Fig. 2.

We tried to reproduce the window transmission by using Eqn (2). To this purpose, we assume that the 300 nm polymer layer is composed by polyvinyl formal resine, known as its originally registered trade name Formvar®. The mass concentrations of the polymer are: 69% C, 3% H, 21% O, and 7% N, and its density is 1.4 g/cm³. According to Scholze and Procop[6] and to Trincavelli *et al.*,[18] the window has boron and aluminum. Bearing this in mind, we also included a boron hydride layer of 20 nm[18] and an aluminum layer in the calculation. This aluminum layer is used for charge dissipation and for preventing the entrance of UV, IR, and visible radiation.[17] Because of the lack of the thickness value, we used it as an adjustable parameter to fit the transmission curve. A good agreement was obtained with an aluminum thickness in the range between 30 and 38 nm, slightly larger than the value obtained by Scholze and Procop.

The intrinsic efficiency of the detector can be estimated by multiplying the window transmission by the QE. The result of our calculations with Eqn (1–3) is shown in Fig. 3.

The purpose of this work was to study experimentally the efficiency of our detector in a wide energy region, especially for energies below 1 keV and over 10 keV, where a decreasing
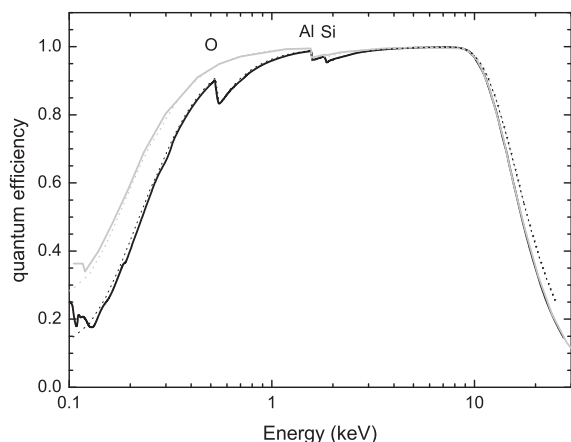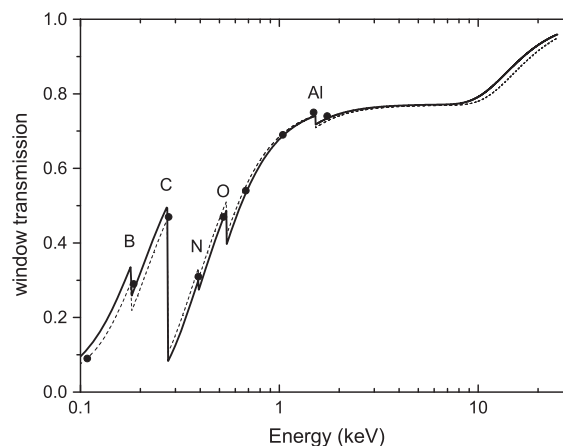

Figure 1. Detector quantum efficiency (QE) as a function of the X-ray energy. QE provided by the manufacturer corresponding to a detector with a pn entrance layer (black solid line) and with a standard entrance layer (gray solid line), QE for a standard entrance layer obtained from Eqn (3) (gray dashed line) and results obtained with Eqn (3) adding a SiO_2 layer of 9 μg/cm² (black dashed line).

Figure 2. AP3.3 window transmission as a function of the X-ray energy. Solid line: curve obtained by Scholze and Procop by fitting experimental data,[6] circles: data given by the supplier,[17] dashed line: Eqn (2) assuming that the polymer is composed by Formvar, a layer of boron hydride and a layer of Al (38 nm).

Table 1. Emission lines at energies E_b and E_a used in Eqn (6). The corresponding X-ray characteristic energies (in keV) are shown between parenthesis

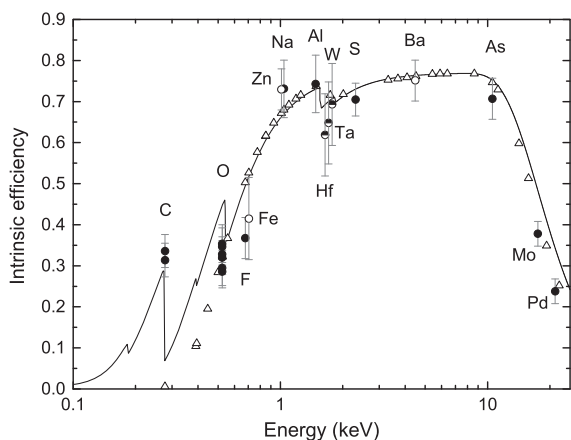| Compound or element	E_b	E_a
NaAlSi$_3$O$_2$	Si-K (1.774)	O-K (0.525), Na-K (1.041), Al-K (1.487)
SiO$_2$	Si-K (1.774)	O-K (0.525)
Al$_2$O$_3$	Al-K (1.487)	O-K (0.525)
CaCO$_3$	Ca-Kα (3.692)	C-K (0.277), O-K (0.525)
CaF$_2$	Ca-Kα (3.692)	F-K (0.677)
GaAs	Ga-Kα (9.252)	As-Kα (10.521)
FeS$_2$	Fe-Kα (6.404)	S-Kα (2.308), Fe-Lα (0.705)
Fe$_3$O$_4$	Fe-Kα (6.404)	O-Kα (0.525)
ZnS	Zn-Kα (8.634)	S-Kα (2.308)
BaSO$_4$	S-Kα (2.308)	O-K (0.525), Ba-Lα (4.457)
Ta	Ta-Lα (8.119)	Ta-Mα (1.710)
Hf	Hf-Lα (7.872)	Hf-Mα (1.645)
W	W-Lα (8.369)	W-Mα (1.775))
Mo	Mo-Lα (2.290)	Mo-Kα (17.427)
Pd	Pd-Lα (2.833)	Pd-Kα (21.104)

Figure 3. Intrinsic efficiency of the SDD as a function of the X-ray energy. Circles: values obtained from the X-ray emission spectra of K (filled circles), L (open circles), and M-lines (half filled circles); solid line: efficiency from Eqn (1); triangles: values given by GUPIX for the detector with AP3.3 window.

behavior is expected. Then, the efficiency ε_a for some discrete energies E_a were obtained with Eqn (6), normalizing the efficiency values ε_b at energies E_b to the estimated efficiency curve. We selected energies E_b in the region between 1 and 10 keV, where the estimated efficiency remains almost constant. In Table 1, we specify, for each compound or element measured, the selected emission lines. The X-ray intensities I_j involved in Eqn (6) were obtained from the measured spectra and the X-ray yields Y_j were calculated with the Thin/Thick/Multi-Layered Target X-ray Yield program (GUYLS application) included in the GUPIX package. The database implemented in this program is detailed by Campbell et al.[19] In Fig. 3, we show the obtained efficiencies ε_a.

The uncertainties in the efficiency values calculated with Eqn (6) were estimated by considering the uncertainties in the quantities involved. The error associated to the counting statistics is negligible because calculations were performed with intensities corresponding to major elements. Uncertainties in the X-ray

yields were estimated from uncertainties in the fluorescence yields, relative transition probabilities, ionization cross sections, and vacancy production cross sections. According to Campbell,[20] a reasonable value for the uncertainties of fluorescence yields for the K-shell are 8%, 5%, and 3% for elements with $Z < 7$, $6 < Z < 17$, and $Z < 16$, respectively. Relative errors of 3% and 5% were assumed, respectively, for the fluorescence yields corresponding to L_3 and M_5 subshells (involved in $L\alpha$ and $M\alpha$ X-ray main transitions).[21,22] The uncertainties related with relative transition probabilities were estimated to be 2% for $K\alpha$ and 3% for $L\alpha$ and $M\alpha$ transitions.[20,23] The uncertainties in ionization cross section for the K-shell are 3%, and the errors of the cross sections for vacancy production (including Coster–Kronig transitions) are assumed to be 5% and 7% for L and M shells, respectively.[19,22,24]

As can be seen in Fig. 3, the efficiency obtained from M lines has larger uncertainties due to the great dispersion of atomic data related to the M shell.[20] On the other hand, the accuracy in the estimation of the efficiency by using Na-$K\alpha$ transition is affected because of the tendency of sodium to migrate from the sample when forming a solid solution (as in the case of NaAlSi$_3$O$_8$).[24]

The behavior of the efficiency with the photon energy can be divided in three zones. For energies lower than 1 keV, the efficiency decreases and presents abrupt jumps for the ionization energies of the elements composing the entrance window. The window transmission T_{win} is the dominating factor of the efficiency in this zone. For energies between 3 and 10 keV, the efficiency remains almost constant, approximately equal to the open area fraction of the supporting grid. Photons with energies higher than 10 keV have enough energy to escape from the detector and, consequently, the efficiency decreases.

The efficiency estimated by the GUPIX software for an SDD with the AP3.3 window is included in Fig. 3 for comparison.[19] Although this software uses the window transmission values of Scholze and Procop,[6] the efficiency values below 0.6 keV are lower than our estimations. In the case of C-$K\alpha$, GUPIX assesses the efficiency at an energy higher than C absorption edge, underestimating the efficiency for this line.

In order to evaluate the consistency of the efficiency values obtained in the present work, an X-ray spectrum from a sample with known composition was quantified. The spectrum was processed with the GUPIX software. We obtained the elemental mass concentrations for two efficiency data sets. On the one hand, we used the efficiency values obtained with Eqn (6), except the ones corresponding to M-lines because they have large uncertainties. For the energies where two or more values were available, the average of the efficiency was used. On the other hand, we used the efficiency values estimated with Eqn (1). In all cases, the geometric factor H involved in the efficiency was set equal to the nominal solid angle subtended by the detector. The fractional mass concentrations resulting from these analyses are shown in Table 2, whereas the measured spectrum and the final fit are shown in Fig. 4. The uncertainties corresponding to the nominal values where estimated

taking into account the detection limits reported by Actlabs for the technique used in the quantification.

Uncertainties in mass concentrations were estimated taking into account the counting statistic, the fitting error evaluated by the GUPIX software, and the uncertainty in the detector efficiency. The first two error sources are the most important for minor and trace elements. The uncertainties for the efficiency values obtained with Eqn (6) were estimated to be 7% for C, 8% for O, 9% for X-ray energies in the range 0.6 keV $E < 1.5$ keV, 7% for 1.6 keV $< E < 10.5$ keV, and 10% for $E > 10.6$ keV. In the case of the efficiency calculated with Eqn (1), the uncertainties were estimated by considering the error of the mass absorption coefficients given by Chantler et al.[16] This estimation leads to errors of around 10% for C-K and O-K lines, 2% for X-ray energies in the range 1 keV $< E < 10$ keV, and 4% for energies larger than 10 keV.

For most elements, the results obtained by using the detector efficiency determined experimentally [Eqn (6)] are closer to the nominal values than those obtained with the calculated efficiency [Eqn (1)]. Both methods underestimated the phosphorus content. In addition, we detected trace amounts of chlorine not present in the nominal concentrations. We note that, because of the uncertainty in the efficiency at low energies, the concentrations of carbon and oxygen present high errors that are typical for minor and trace elements.

Table 2. Fractional mass concentrations obtained with the efficiency values determined with Eqn (6) (Model 1) and with Eqn (1) (Model 2). Numbers in parenthesis are the estimated uncertainties in the last digits

	Mass concentrations		
Z	Nominal[a]	Model 1	Model 2
C	0.0188 (3)	0.0185 (21)	0.0216 (31)
O	0.4746 (1)	0.470 (41)	0.414 (43)
Na	0.01758 (8)	0.0172 (18)	0.0194 (23)
Mg	0.00736 (6)	0.0091 (10)	0.0100 (12)
Al	0.09506 (5)	0.108 (10)	0.1162 (28)
Si	0.30931 (5)	0.297 (28)	0.330 (8)
P	0.00170 (4)	0.00116 (33)	0.0012 (3)
Cl	—	0.00084 (18)	0.00094 (20)
K	0.03511 (8)	0.0369 (30)	0.0414 (13)
Ca	0.01472 (7)	0.0143 (13)	0.0161 (7)
Ti	0.002146 (6)	0.00194 (29)	0.00210 (20)
Mn	0.000290 (8)	0.00022 (17)	0.00023 (18)
Fe	0.02322 (7)	0.0254 (24)	0.0271 (12)

[a]The nominal concentrations were determined by Actlabs.[15]

Summary

We have studied the efficiency of an SDD with the aim to characterize its behavior mainly at low X-ray energies. Our calculation of the QE showed a good agreement with data provided by the manufacturer when the named pn entrance window is represented by an additional silicon oxide layer of appropriate thickness. For the AP3.3 ultrathin polymer window, we could obtain a transmission curve as a function of the X-ray energy close to the curve given by Scholze and Procop,[6] and also to the data from the supplier. Then, the detector efficiency was calculated as the product of the QE and the window transmission. In this case, the main error source is related with the uncertainties in mass absorption coefficients. Additionally, we obtained experimental values of the efficiency from measured X-ray spectra for samples of known composition. As the results refer to relative efficiency values taken at two X-ray energies, a normalization procedure was necessary.

The quantification of a reference sample showed that the efficiency values estimated from measured spectra led to fractional mass concentrations in good agreement with the nominal sample composition. Moreover, this method allowed us to assess the uncertainties in the sample composition by means of experimental data.
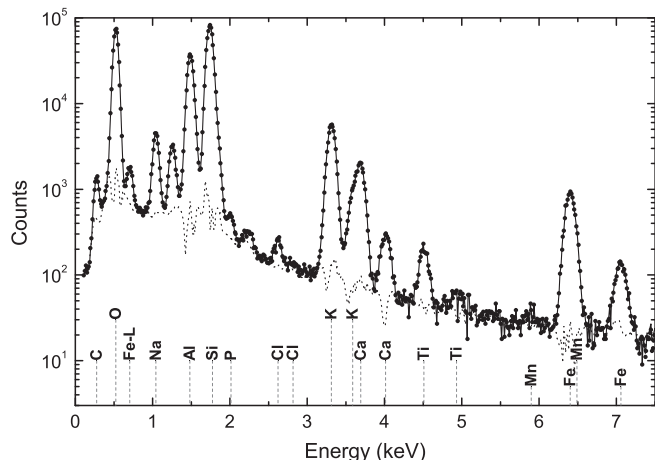

Figure 4. Experimental spectrum (dots), final fit (solid line), and background (dotted line) obtained with GUPIX for the reference sample.

References

[1] E. Gatti, P. Rehak. *Nucl. Instr. Meth. Phys. Res. A* **1984**, *225*, 608.

[2] P. Lechner, C. Fiorini, A. Longoni, G. Lutz, A. Pahlke, H. Soltau, L. Strüder. *Adv. X-ray Anal.* **2004**, *47*, 53.

[3] R. Hartmann, D. Hauff, P. Lechner, R. Richter, L. Strüder, J. Kemmer, S. Krisch, F. Scholze, G. Ulm. *Nucl. Instr. Meth. Phys. Res. A* **1996**, *377*, 191.

[4] R. Hartmann, L. Strüder, J. Kemmer, P. Lechner, O. Fries, E. Lorenz, R. Mirzoyan. *Nucl. Instr. Meth. Phys. Res. A* **1997**, *387*, 250.

[5] D. M. Schlosser, P. Lechner, G. Lutz, A. Niculae, H. Soltau, L. Strüder, R. Eckhardt, K. Hermenau, G. Schaller, F. Schopper, O. Jaritschin, A. Liebel, A. Simsek, C. Fiorini, A. Longoni. *Nucl. Instr. Meth. Phys. Res. A* **2010**, *624*, 270.

[6] F. Scholze, M. Procop. *X-Ray Spectrom.* **2005**, *34*, 473.

[7] J. Tschischgale, D. Kichler, U. Lehnert, G. Zschornack. *Nucl. Instr. Meth. Phys. Res. A* **1997**, *400*, 387.

[8] L. C. Tribedi, P. N. Tandon. *Nucl. Instr. Meth. Phys. Res. B* **1992**, *69*, 178.

[9] F. Scholze, G. Ulm. *Nucl. Instr. Meth. Phys. Res. A* **1994**, *339*, 49.

[10] M. Alvisi, M. Blome, M. Griepentrog, V. D. Hodoroaba, P. Karduck, M. Mostert, M. Nacucchi, M. Procop, M. Rohde, F. Scholze, P. Statham, R. Terborg, J. F. Thiot. *Microsc. Microanal.* **2006**, *12*, 406.

[11] S. J. B. Reed, N. G. Ware. *J. Phys. E: Sci. Instrum.* **1972**, *5*, 582.

[12] S. A. E. Johansson, J. L. Campbell, K. G. Malmqvist, Particle-Induced X-Ray Emission Spectrometry (PIXE), John Wiley & Sons, New Jork, **1995**.

[13] B. P. Mohanty, P. Balouria, M. L. Garg, T. K. Nandi, V. K. Mittal, I. M. Govil. *Nucl. Instr. Meth. Phys. Res. A* **2008**, *584*, 186.

[14] M. Budnar, J. Campbell, S. Fazinic, M. Jakšic, A. Kobzev, A. Kótai, W. Lanford, I. Orlic, F. Pászti, E. Rauhala, A. Turos, Instrumentation for PIXE and RBS IAEA-TECDOC-1190 ISSN 1011–4289, IAEA Vienna, Australia, **2000**.

[15] www.actlabs.com

[16] C. T. Chantler, K. Olsen, R. A. Dragoset, J. Chang, A. R. Kishore, S. A. Kotochigova, D. S. Zucker, **2005**. X-ray Form Factor, Attenuation and Scattering Tables Version 2.1. Gaithersburg, MD: National Institute of Standards and Technology. Available at: http://physics.nist.gov/ffast -accessed on October 23, 2012. Originally published as C. T. Chantler, *J. Phys. Chem. Ref. Data* **2000**; 29, 597 and C. T. Chantler, *J. Phys. Chem. Ref. Data* **1995**; 24, 71.

[17] J. Trincavelli, S. Limandri, A. Carreras, R. Bonetto. *Microsc. Microanal.* **2008**, *14*, 306.

[18] J. L. Campbell, N. I. Boyd, N. Grassi, P. Bonnick, J. A. Maxwel. *Nucl. Intr. Meth. Phys. Res. B* **2010**, *268*, 3356.

[19] J. Campbell, A Report Prepared for the International Initiative on X-ray Fundamental, University of Canberra, http://www.canberra.edu.au/irps/archives/vol24no1/xray.pdf (accessed October 1, 2012).

[20] D. C. Joy. *Microsc. Microanal.* **2001**, *7*, 159.

[21] J. L. Campbell. *At. Data Nucl. Data Tables* **2003**, *85*, 291.

[22] S. Limandri, J. Trincavelli, R. Bonetto, A. Carreras. *Phys. Rev. A* **2008**, *78*, 022518.

[23] J. L. Campbell, T. L. Hopman, J. A. Maxwell, Z. Nejedly. *Nucl. Instr. Meth. Phys. Res. B* **2000**, *170*, 193.

[24] D. M. Usher. *J. Phys. C: Solid State Phys.* **1981**, *14*, 2039.